Contact forces between a particle and a wet wall at both quasi-static and dynamic state

Huang Zhang[1], *Sheng* Chen[1], and *Shuiqing* Li[1,*]

[1]Key Laboratory of the Thermal Science and Power Engineering of Ministry of Education, Department of Thermal Engineering, Tsinghua University, Beijing 100084, China

Abstract. The contact regime of particle-wall is investigated by the atomic force microscope (AFM) and theoretical models. First, AFM is used to measure the cohesive force between a micron-sized grain and a glass plate at quasi-static state under various humidity. It is found out that the cohesive force starts to grow slowly and suddenly increase rapidly beyond a critical Relative Humidity (RH). Second, mathematical models of contacting forces are presented to depict the dynamic process that a particle impacts on a wet wall. Then the energy loss of a falling grain is calculated in comparison with the models and the experimental data from the previous references. The simulation results show that the force models presented here are adaptive for both low and high viscosity fluid films with different thickness.

1 Introduction

Wet granular materials are most common in our daily environment as well as in many engineering processes [1,2]. The packing or flow behaviour of wet granular media is closely relevant with the interactions at the grain level [1]. Interstitial liquid between the wet grains induces the granular matter cohesive arising from the capillary forces [3]. The experimental measurements and theoretical derivation to determine the magnitude of capillary force between Geldart-D coarse particles have been well established at quasi-static state [3-5]. For micron-sized grains, other adhesion effects caused by van der Waals force, electrostatic force, etc., become significant and complex [6]. So it is interesting to investigate how capillary force behaves in such a small length-scale. It seems that AFM offers a '*prototypical*' approach to measure the contact forces in these conditions [7].

When the wet granular media is agitated, partially wetted grains are impacting and separating with each other [8]. The thin liquid layer covering a wet grain helps to push or pull the other grain [8]. Due to the hydrodynamic and viscous fluid flows in this liquid film, the first-contact energy loss [9] of wet particles is higher than that of dry ones [10]. Experiments can determine the particle velocities before and after collisions, so that the first-contact energy loss is obtained according to the velocity differences [10]. However, the details of contact mechanism of wet particles are relied on the theoretical analysis [11].

The structure of this paper is organized as following. First, the capillary force between a micron-sized grain and a plate (the plate can be considered as a sphere with zero curvature) is measured by AFM under different humidity. Second, the force models of a grain colliding with a wet wall are established in order to analyze the contacting mechanism, especially the first-contact energy loss between the grain and the wet wall.

2 Experiment setup

Fig. 1 shows the humidity control system and AFM (CSPM5500) setup. The circuit of nitrogen flows going through the water tank is to entrain liquid into the AFM cell, while another circuit of dry nitrogen is to control the magnitude of RH. The RH in AFM cell is adjusted to range from 2% to 85%. RH is measured by VAISALA sensor. A SiO_2 particle with diameter 15.52 μm is glued to the original AFM tip to form a spherical tip.

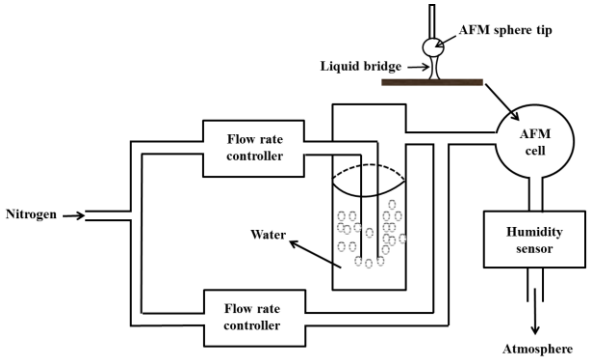

Fig. 1. Humidity control system and AFM setup.

3 Theoretical models

This part focuses on the establishing of the dynamic model that a grain impacts on a wet wall. Fig.2 performs

* Corresponding author: lishuiqing@tsinghua.edu.cn

the penetration and rebound schematic diagram. In this figure, β is the angle between the three-phase contact line and the y axis, and θ is the contact angle of solid and liquid. When the falling particle contacts the liquid layer (stage I), the fluids are draining out in the thin gap. During this process, the particle undergoes the resistance from the surface integration of the fluid stress at the interface between the particle and the liquid layer [12]. After penetrating the liquid film, the grain is colliding with the wall (stage II), and then, the grain rebounds through the fluid layer (stage III). After that, the liquid bridge pulls the particle until it is ruptured.

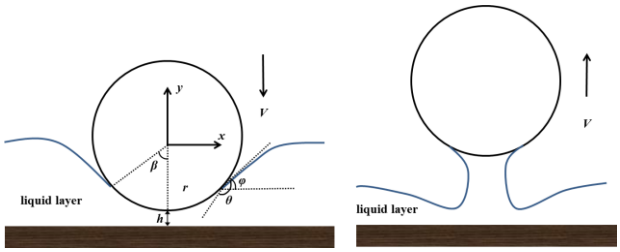

Fig. 2. Schematic diagram of a particle penetrating and separating with a liquid layer.

In stage I, the particle undertakes gravity force, surface tension force and the fluid force resulting from the fluid flows in the thin layer. This fluid force consists of three parts: unsteady, buoyance and resistance term [11,12]. When the particle Reynolds number Re_p is sufficiently small, the buoyance and resistance terms are converted into the lubrication force [3, 11]. The motion equation of the sphere at this stage is shown as below

$$m_p \frac{d\boldsymbol{v}}{dt} = \boldsymbol{F}_g + \boldsymbol{F}_s + \boldsymbol{F}_a + \boldsymbol{F}_b + \boldsymbol{F}_d, \qquad (1)$$

where m_p, $\boldsymbol{v}$, $\boldsymbol{F}_g$, $\boldsymbol{F}_s$, $\boldsymbol{F}_a$, $\boldsymbol{F}_b$ and $\boldsymbol{F}_d$ are particle mass, particle velocity, gravity force, surface tension force, unsteady force, buoyance force and drag force, respectively. These forces are expressed as: $\boldsymbol{F}_g = (4/3)\pi r^3\boldsymbol{g}$, $\boldsymbol{F}_s = -2\pi\gamma r\sin\beta\sin\varphi\boldsymbol{v}/|\boldsymbol{v}|$, $\boldsymbol{F}_a = -(1/6)\pi r^3\rho_f(\cos^3\beta - 3\cos\beta+2)\mathrm{d}\boldsymbol{v}/\mathrm{d}t$, $\boldsymbol{F}_b = -(1/3)\pi r^3\rho_f(2+\cos\beta)(1-\cos\beta)^2\boldsymbol{g}$, $\boldsymbol{F}_d = -(1/2)\pi C_d\rho_f(r\sin\beta)^2|\boldsymbol{v}|\boldsymbol{v}$, where r, $\boldsymbol{g}$, γ, ρ_f, and C_d are particle radius, gravity acceleration, surface tension coefficient, liquid density, and drag coefficient, respectively [11,12]. C_d is related with Re_p, which are defined as below [11]

$$C_d = \frac{24}{\mathrm{Re}_p} + \frac{4}{\sqrt{\mathrm{Re}_p}} + 0.4, \mathrm{Re}_p = \frac{\rho_f |\boldsymbol{v}| d}{\mu}, \qquad (2)$$

where d, μ are particle diameter and liquid viscosity. Particularly, if the flow Reynolds number Re_f in the liquid film is small, buoyance force and drag force are eventually lubrication force [3,13]. Re_f, which is estimated by considering mass conservation in the liquid layer, is performed as $\mathrm{Re}_f = \rho_f|\boldsymbol{v}|(rh)^{0.5}/(2\mu)$, where h is the gap distance between the bottom of sphere and the wall [3]. Here, we assume that if Re_f is less than one, $\boldsymbol{F}_b$ and $\boldsymbol{F}_d$ become to be the lubrication force $\boldsymbol{F}_l$, which is shown as $\boldsymbol{F}_l = -6\pi\mu r^2|\boldsymbol{v}|/(h+h_r)$ [11]. Here h_r is the surface roughness, which is used to avoid the physical singularity when h is approaching zero [14].

In stage II, the grain collides with the wall with no interstitial fluid evolves any more [10]. We use $\boldsymbol{v}_1$ and $\boldsymbol{v}_2$ to represent the particle velocities that are just contacting and leaving the wall surface. Therefore, $\boldsymbol{v}_1$ and $\boldsymbol{v}_2$ are correlated with the restitution coefficient between the particle and the dry wall [6,10], which is given as $\boldsymbol{v}_2 = -e_{\mathrm{dry}}\boldsymbol{v}_1$, where e_{dry} is the restitution coefficient for dry condition.

In stage III, the grain starts to leave the wet wall. The forces that the particle undergoes in this period are nearly the same as those in stage I. While, $\boldsymbol{F}_s$ is replaced by the liquid bridge force $\boldsymbol{F}_c$ [4], which is given as below

$$\boldsymbol{F}_c = -2\pi\gamma r\cos\theta\left(1 - \frac{1}{\sqrt{1+\frac{2V_b}{\pi r(h+h_r)^2}}}\right)\frac{\boldsymbol{v}}{|\boldsymbol{v}|}. \qquad (3)$$

V_b is the liquid bridge volume, which is estimated as $d^3/16$ [10]. The rupture distance h_{rup} is crucial to determine the breaking point of the liquid bridge. The evolution of h_{rup} is expressed as [5]

$$h_{\mathrm{rup}} = (1+\theta)(1+\sqrt{\mathrm{Ca}})V_b, \qquad (4)$$

where Ca is the capillary number that equals to $\mu|\boldsymbol{v}|/\gamma$. Otherwise, β and θ keep constant where $\beta = 120^o$ [16] and $\theta = 111^0$ [15] in stage I, and, $\beta = 80^o$ [16] and $\theta = 10^0$ [17] in stage III. Additionally, φ equals $\beta+\theta-\pi$ [12].

4 Results and discussions

Fig. 3 gives the AFM measurement of the critical cohesive force F_{crit} under different RH. In general, the magnitude of F_{crit} grows with increasing RH. F_{crit} rises slowly when RH is below the critical RH that is around 65%. While, F_{crit} rises up rapidly as RH is beyond 65%. Actually, the surfaces of both SiO_2 particle and glass plate are not smooth (the average roughness is about 2.98 nm by AFM measurement). As RH ranges from 3% ~ 65%, liquid could only exist within the surface concave due to capillary condensation [7]. Hence, the liquid connections can hardly contribute to the increment of the total cohesive force. When RH is high (beyond 65% in this case), still due to the capillary condensation, liquid could fill up the gap between the micron-sized particle and the plate. Then, the liquid volume V_b in the gap rises with the growing RH. Because the distance between the particle and the wall is constant, F_{crit}, which is now estimated by Eq. (3) [4,7], would become larger and larger with increasing V_b.

The occurrence of critical RH needs further analysis. In equilibrium state, Kelvin equation describes the relationship between the shape of liquid concave and RH, which is shown as below,

$$r_c = \frac{2\gamma V_m}{R_g T\log(\mathrm{RH})}, \qquad (5)$$

where r_c, γ, V_m, R_g, and T are liquid concave radius, surface tension, liquid molar volume, ideal gas constant, and temperature. When the condensate liquid just fills up the surface roughness, r_c is estimated as -2.98 nm, whose magnitude is supposed to be the average roughness. We take T as 20°C, so RH is calculated as 69.6% by Eq. (5), which is very close to the critical RH (65%) from Fig. 3. Further, suppose the gap between the particle and the plate is filled with liquid if RH is approaching to 90% or higher. The contact force is regarded as $F_{crit} \sim \pi\gamma d$ [3]. According to the material properties, $F_{crit} \sim \pi\times73\times10^{-3}\times15.52\times10^{-6}$ N ~ 3600 nN, which is more or less close to the maximum value of F_{crit} (about 2000 nN) in Fig. 3.

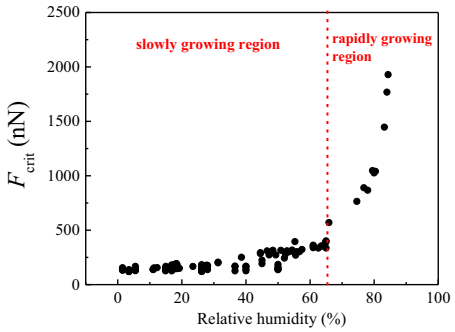

Fig. 3. Critical cohesive force F_{crit} increases with relative humidity by AFM measurement.

Eq. (1) quantitatively capture the essential features of the impacting process in Fig. 2. In stage I, the total distance that the grain moves is the initial thickness of liquid layer δ. Substituting the impacting velocity of particle $\boldsymbol{v}_0$ into Eq. (1), we can get $\boldsymbol{v}_1$ after numerically solving this Ordinary Differential Equation (ODE, and the numerical toolkit used here is ODE45 in MATLAB R2010a). Then, $\boldsymbol{v}_3$ is also obtained from Eq. (1), in which $\boldsymbol{F}_s$ is instead of $\boldsymbol{F}_c$. Therefore, the first-contact energy loss is expressed as $0.5m_p(|\boldsymbol{v}_0|^2 - |\boldsymbol{v}_3|^2)$. In order to verify these theoretical models, ΔE_{wet} that indicates the energy loss during the process of the grain interacting with the liquid film, is compared with the experimental data in reference [10]. Obviously, ΔE_{wet} equals to $0.5m_p(|\boldsymbol{v}_0|^2 - |\boldsymbol{v}_3|^2 - |\boldsymbol{v}_2|^2 + |\boldsymbol{v}_1|^2)$. Meanwhile, according to an energy budget analysis referred in ref. [10], ΔE_{wet} mainly consists of viscous dissipation and fluid material acceleration, which are given by [10]

$$\Delta E_{wet} = \Delta E_{vis} + \Delta E_{acc}, \tag{6}$$

$$\Delta E_{vis} = \frac{3}{2}\pi\mu d^2 \,|\, \boldsymbol{v}_0 \,|\, (\ln\frac{\delta}{h_r} + \ln\frac{h_{rup}}{h_r}), \tag{7}$$

$$\Delta E_{acc} = \frac{3\rho_f}{2\rho_s}(\frac{\delta}{d} - \frac{3}{5}(\frac{\delta}{d})^2 + \frac{2}{3}(\frac{\delta}{d})^3)m_p v_0^2. \tag{8}$$

Here d_{rup} is considered as $2d$ according to the observation in ref. [10]. The material properties of two kinds of fluid M5 and M50 are given in Table 1. The restitution coefficient e_{dry}, particle roughness h_r, particle density ρ_s and diammeter d are 0.985, 5 μm, 2580 kg/m^3 and 5.5 mm, respectively [10].

Table 1. The material properties of M5 and M50 [10].

Liquid	ρ_f (kg/m^3)	γ (mN/m)	μ (mPa·s)
M5	925	19.2	4.6
M50	965	20.8	48

As seen in Fig. 4(a), ΔE_{wet} predicted by our models is in good agreement with the experimental data. Generally, ΔE_{wet} increases with $|\boldsymbol{v}_0|$. Also, the more thick δ is, the larger ΔE_{wet} is dissipated. Remarkably, the energy loss of the particle impacting into the liquid M50 is much higher than that of the liquid M5. For instance, ΔE_{wet} is around 20 μJ as $|\boldsymbol{v}_0|$ is 1 m/s in the liquid M5 case, which is nearly one third of that in the same case of liquid M50.

Although the results obtained from Eqs. (6-8) qualitatively follow the tendency of ΔE_{wet} versus $|\boldsymbol{v}_0|$ and δ, it deviate a lot in case of liquid M5. However, the accuracy of Eqs. (6-8) is highly promoted when calculating ΔE_{wet} in liquid M50. In contrast, ΔE_{wet} obtained by our model can still agree well with the experimental data of liquid M50, but they are not as well as the results by Eqs. (6-8) in this case. The viscosity of liquid M50 is nearly one thousand times larger than M5. Eq. (7) can be considered as the intergration of $\boldsymbol{F}_l$, which is given as below

$$\Delta E_{vis} = \int_{h_r}^{d_{rup}} + \int_{\delta}^{h_r} (\boldsymbol{F}_l \cdot d\boldsymbol{x}) = \int_{h_r}^{d_{rup}} + \int_{\delta}^{h_r} (\frac{3\pi\mu d^2 \boldsymbol{v}}{2x} \cdot d\boldsymbol{x}). \tag{9}$$

Eq. (7) is obtained from integrating Eq. (9) by taking $\boldsymbol{v}$ as $\boldsymbol{v}_0$, which should be larger than the particle velocity in actual situation. This is the reason that Eqs. (6-8) could get good results in the viscosity dominated case (M50), but fail in the less viscosity case (M5). However, as seen from Fig. 4, our model is adaptive for both low and high viscosity fluid. Furthermore, our model could predict the particle velocity at any given time, which is convenient to analysis the contacting mechanism of the particle with the liquid layer.

Fig. 4 indicates that ΔE_{wet} depends on $\boldsymbol{v}_0$, μ, and δ, etc. A usually used dimensionless numer to clarify the energy loss process is Stokes numer St, which is defined as $\rho_s d|\boldsymbol{v}_0|/(9\mu)$ [3,10-11,13]. In the main diagram of Fig. 5, the experimental points of $\Delta E_{wet}/E_0$ (E_0 is the initial kinetic energy of an impact particle) are almost collapsed into a fitting curve, whose form is as $a\mathrm{St}^{-2}+b\mathrm{St}^{-1}+c$. Similarly, the scatter results by our model are also fitted by a curve with the same form as in the main diagram.

As seen in Fig.5, the ratio of ΔE_{wet} to E_0 does not exceed 0.4 when St^{-1} ranges from 0 to 0.005. With increasing St^{-1}, this ratio grows up to around 0.8. The law of the fitting curve is not occasional, which is intrinsically shown as following: $\Delta E_{wet}/E_0$ is direct propotion to e_n^2 [10], where e_n is the coefficient of

restitution. Further, $e_n \sim (1\text{-St}^{-1})$ [3] to lead that the curve of $\Delta E_{wet}/E_0$ is in the form of $a\text{St}^{-2}+b\text{St}^{-1}+c$.

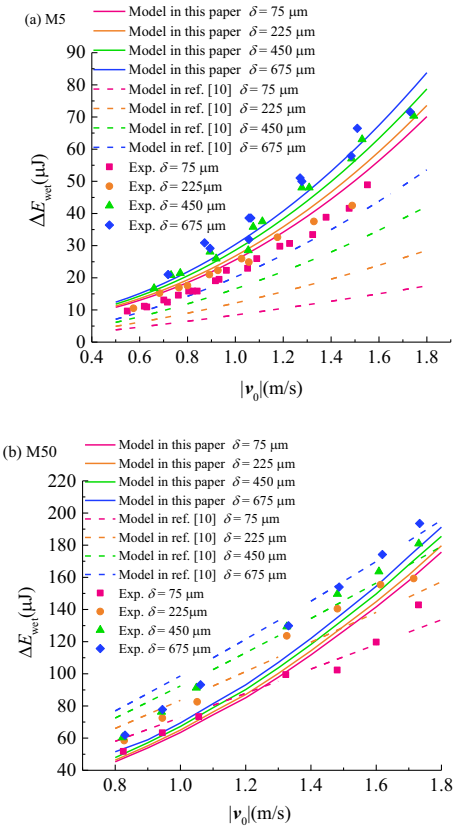

Fig. 4. ΔE_{wet} caclulated by the model in this paper is compared with both the model as shown in Eqs. (6-8) and experimental data in reference [10].

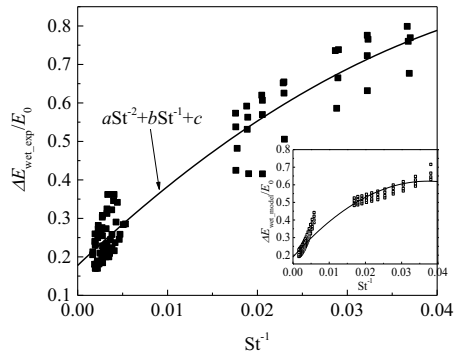

Fig. 5. The ratio of ΔE_{wet} to E_0 varies with St^{-1} by experiment in reference [10] (inset is the result predicted by our theoretical model).

5 Conclusions

In this paper, the forces that the particle contacts with a wet wall in both quasi-static and dynamic state are performed. First, capillary force is measured by AFM between a micron-sized particle and a glass plate. It is found out that the capillary force begins to grow slowly with RH, and then increases rapidly. This result is explained by capillary condensation that liquid only exists in the concave of the surface roughness below a critical RH, but it fills up the gap beyond a critical value.

Second, the colliding process that a falling grain impacting onto a wet wall is analyzed. Compared with the methodology of energy budget referred in the previous literature, the force models presented here could not only calculate the first-contact energy loss, but also study the contact forces and particle velocities at any given time. The simulation results show that our model agrees well with the experimental data and are adaptive in both low and high viscosity fluid cases.

Acknowledgements

This work was funded by the China Postdoctoral Science Foundation and the Major State Basic Research Development Program of China (Grant No. 2016YFC0203705).

References

1. S. Herminghaus, Adv. Phys. **54**, 221 (2005).
2. J. Delenne, V. Richefeu, F. Radjai, J. Fluid Mech. **762**, R5 (2015).
3. B. Andreotti, Y. Forterre, O. Pouliquen, *Granular media between fluid and solid* (Cambridge University Press, New York, 2013).
4. O. Pitois, P. Moucheront, X. Chateau, J. Colloid Interface Sci. **231**, 26 (2000).
5. O. Pitois, P. Moucheront, X. Chateau, Eur. Phys. J. B **23**, 79 (2001).
6. J. Marshall, S. Li, *Adhesive particle flow a discrete-element approach* (Cambridge University Press, New York, 2014).
7. R. Jones, H. Pollock, J. Cleaver, C. Hodges, Langmuir **18**, 8045 (2002).
8. P. Liu, R. Yang, A. Yu, Chem. Eng. Sci. **86**, 99 (2013).
9. S. Chen, S. Li, M. Yang, Powder Technol. **274**, 431 (2015).
10. F. Gollwitzer, I. Rehherg, C. Kruelle, K. Huang, Phys. Rev. E **86**, 011303 (2012).
11. S. Antonyuk, S. Heinrich, N. Deen, H. Kuipers, Particuology **7**, 245 (2009).
12. D. Lee, H. Kim, Langmuir **24**, 142 (2008).
13. J. Simeonov, Acta. Mech. **227**, 565 (2016).
14. E. Izard, T. Bonometti, L. Lacaze, J. Fluid Mech. **747**, 422 (2014).
15. D. Vella, Langmuir **22**, 2972 (2006).
16. A. Wang, Q. Song, Q. Yao, Atmos. Environ. **115**, 1 (2015).
17. R. Zhu, S. Li, Q. Yao, Phys. Rev. E **87**, 022206 (2013).